Geometrical Framework for Hydrodynamics and Control of Wave Energy Converters

Alexis Mérigaud, Benjamin Thiria, Ramiro Godoy-Diana

Geometrical Framework for Hydrodynamics and Control of Wave Energy Converters

Alexis Mérigaud,[*] Benjamin Thiria,[†] and Ramiro Godoy-Diana[‡]
Laboratoire de Physique et Mécanique des Milieux Hétérogénes (PMMH), CNRS UMR 7636, ESPCI Paris—PSL University, Sorbonne Université, Université Paris Cité, Paris 75005, France

(Received 30 September 2022; revised 18 March 2023; accepted 27 March 2023; published 3 May 2023)

This article presents a simple geometrical approach to visualize the hydrodynamic properties of wave energy converters (WECs), in terms of wave reflection, transmission, and absorption, and how those properties are governed by the WEC control parameters. The problem is modeled as an array of periodic rows of WECs parallel to the wave front, which is representative of WEC farms located along the shoreline, and allows for a straightforward two-dimensional analysis of energy fluxes. The WECs are assumed to be symmetric with respect to the plane perpendicular to the wave propagation direction, and they operate in a single degree of freedom. Under those assumptions, fundamental hydrodynamic relationships allow the WEC operation at a given frequency to be mapped to a single complex number, $\hat{T}$, which represents the WEC (complex) transmission coefficient, located in a circle with center $1/2$ and radius $1/2$. The WEC hydrodynamic and control parameters (added mass, stiffness, damping) govern the precise location of $\hat{T}$ within the circle. The distance of $\hat{T}$ to the center of the circle determines the hydrodynamic efficiency, between 0 (when $\hat{T}$ is on the circle border) and $1/2$ (which is achieved when $\hat{T}$ is at the center of the circle). Therefore, the representation of $\hat{T}$ provides an immediate insight into the balance between reflection, transmission, and absorption. The proposed unified representation reflects, in a didactic way, some fundamental wave energy concepts, common to all WECs, such as the Haskind relationship, or the impedance matching condition for optimal wave power absorption. Two numerical examples illustrate how the locus of $\hat{T}$, across a prescribed frequency range, provides a distinctive "signature" specific to the WEC geometry, mode of operation, and control strategy. Finally, the proposed representation shows many similarities to the Smith chart and, as such, is but one additional analogy between wave energy conversion and electrical engineering.

DOI: 10.1103/PRXEnergy.2.023003

I. INTRODUCTION

Ocean waves constitute an immense, untapped reservoir of renewable energy. In Europe, for example, wave energy could represent an appreciable contribution to a decarbonized electricity mix, with an estimated capacity potential in the order of 300–400 GW along the Atlantic coastlines alone [1]. Wave energy converters (WECs) will typically be installed in arrays, to reduce the cost per kWh of wave energy, by allowing the mutualization of expenses related to grid connection, infrastructure, installation, and maintenance [2]. In addition to providing clean renewable power, large WEC arrays could contribute to nearshore wave attenuation, thus mitigating coastal erosion [3–6], similarly to the wave reduction effect of natural coastal defenses, such as mangroves, salt marshes, or seagrass and kelp beds [7,8]. More generally, a WEC farm would not only be designed with regard to its wave absorption capabilities—with the potential benefit of improved performance due to collective effects [9]—but also considering the way it will interact with its surroundings. A compelling example was put forward recently by the study of wave power farms acting as artificial reefs, and thus, enhancing biodiversity [10]. In optimizing the array layout, hydrodynamic interaction effects within the WEC farm are crucial, although other factors need to be taken into account, such as connection costs or constraints in terms of space utilization.

Currently a very active research area, power-maximizing control of WECs is seen as another key enabler towards making wave energy economically competitive [11], by

[*]alexis.merigaud@espci.psl.eu; also at IFP Energies Nouvelles
[†]benjamin.thiria@espci.psl.eu
[‡]ramiro.godoy-diana@espci.psl.eu

increasing the average absorbed power while limiting capital costs. Recent years have witnessed the development of a variety of advanced control strategies [12], mostly model based [13], gradually overcoming the main barriers towards achieving optimal power-maximizing WEC control, such as the need for real-time wave force predictions, the computational requirement to solve control optimization problems in real time, the necessity of accounting for nonlinear dynamics, or the robustness of the control strategy to inevitable modeling uncertainties.

Array interaction and control are mutually dependent problems, since optimal control of WECs within an array should take into account array interaction effects, which is termed "coordinated control," [14] while, conversely, the optimal array layout generally depends on the adopted WEC control strategy [15]. Finally, while the optimal control strategy and optimal array layout obviously depend on the characteristics of individual WECs composing the array, the inverse is also true [16], so that, eventually, WEC design, control, and array layout are three interrelated problems.

Even within the scope of linear potential flow theory, WEC hydrodynamics yield mathematically complex problems, even more so when it comes to control and array modeling. In spite of the current advances in computational power and numerical techniques, the study, design, and optimization of WECs and WEC farms can still benefit from analogies with other areas of physics, to understand fundamental concepts behind the initial problem, and to derive simplified models as first approximations. Such analogies have been put to good use since the early years of modern research on wave energy. In particular, Falnes and Budal [17,18] drew powerful parallels with radio-frequency engineering, acoustics, and optics, applying the concept of radiation impedance to WECs and WEC arrays, to derive optimal power-maximizing control conditions, and to explain how wave power can be absorbed over a width significantly larger than the WEC characteristic dimensions. More recently, further electrical equivalents for nonlinear WEC model components were proposed in Ref. [19] and other works by the same authors. Other fruitful analogies arise at the array level, considering the WEC farm as a metamaterial, with properties related to its internal structure, such as the existence of crystallographic effects analogous to those observed in optics, solid-state physics, or acoustics, e.g., Bragg resonances [20–22]. In the broader context of water wave engineering, those ideas are exploited in various systems, such as the refraction phenomena of water waves propagating through an array of bottom-mounted structures [22,23], tuning of the seabed topography [24,25], or the deployment of floating membranes with a crystalline array of defects with the ability to focus water waves in a way similar to optical lenses [26].

This work establishes a relatively simple geometrical representation of wave energy device properties, considering not only power absorption capabilities, but also the WEC interaction with their up-wave and down-wave surroundings. Considering a model assumption of an infinite row of WECs, parallel to the wave front, the row properties in terms of wave reflection, transmission and absorption are represented graphically, depending on the WEC geometry, mode of motion, and control parameters. In fact, the reflection and transmission properties of individual rows, as represented in this paper, can subsequently be used as "building blocks" to solve the array interaction across multiple rows in a straightforward manner [27]. The proposed geometrical representation exhibits strong visual and conceptual resemblance to the Smith chart [28,29], a graphical tool invented by Phillip Smith in the late 1930s, which is well known to radio-frequency engineers for the study of transmission lines [30] and, in particular, impedance matching. Thus, this representation is yet another example in the time-honored tradition of radio-frequencies and electrical analogies in WEC modeling and control. In addition to being a visual help in early modeling stages, encompassing WEC design and control parameters, together with array interaction effects, which may find some practical applications, the framework proposed in this paper is also a didactic way to summarize otherwise well-known fundamental relationships for the two-dimensional analysis of WECs, see e.g., Ref. [31,32].

In Sec. II, the geometrical representation of reflection and transmission coefficients is introduced; first, for devices held fixed or moving freely under the effect of wave forces. However, absorbing power from the waves requires that the power take-off (PTO) system exerts a force onto the WECs, which can be generally decomposed into stiffness, inertia, and damping terms, thus modifying the WEC motion, together with the corresponding reflection and transmission characteristics. Based on the proposed geometrical representation, Sec. III describes how the choice of PTO parameters governs wave reflection, transmission, and power absorption, and examines the relationship between the devices' "wave-making" properties and their wave power absorption capabilities, under motion amplitude limitations. Section IV exemplifies how specific cases can be incorporated into the proposed framework, through two WEC archetypes, namely, flap-type oscillating wave-surge converters and cylindrical heaving point absorbers. Finally, the usefulness and limitations of the present graphical representation, as well as its connections to the Smith chart, are discussed in Sec. V.

II. GEOMETRICAL REPRESENTATION OF TRANSMISSION COEFFICIENTS

A. General assumptions

Consider a body of water with constant depth h of infinite horizontal extent. A Cartesian frame is defined with unit vectors $\vec{e}_x$, $\vec{e}_y$, and $\vec{e}_z$, with the origin located on the

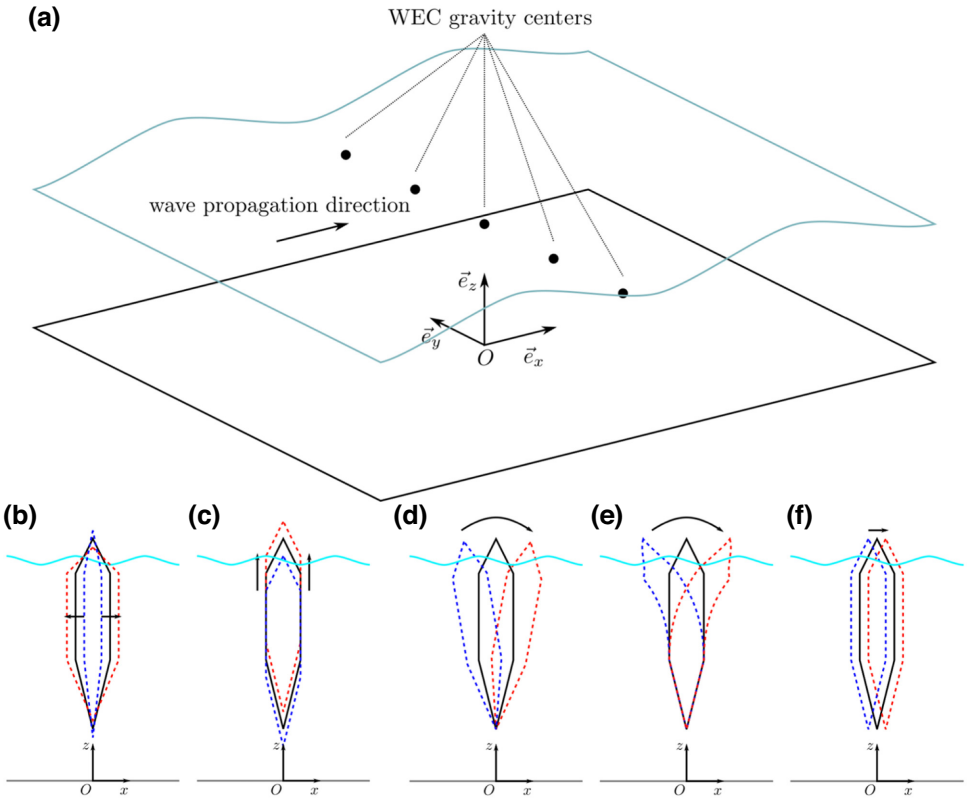

FIG. 1. (a) Layout of the WEC row in the chosen frame of reference. Examples of symmetric modes of motion: (b) inflation, (c) heave. Examples of antisymmetric modes of motion: (d) pitch, (e) flexible deflection, (f) surge.

seabed. WECs are arranged periodically, in an infinitely long horizontal row, in the O-y-z plane without loss of generality. The WEC geometry is assumed to be symmetric with respect to the O-y-z plane. In addition, the WECs operate in either a symmetric or an antisymmetric mode of motion with respect to the O-y-z plane, i.e., the body-normal velocity for an elementary displacement is either symmetric or antisymmetric with respect to the O-y-z plane. Figures 1(b)–1(f) illustrate examples of symmetric and antisymmetric modes of motion, including nonrigid deformations, all encompassed by the present theory.

The fluid and the WECs are harmonically excited by an incident plane wave, propagating in the x direction. Let L be the row transverse periodicity, that is, every pattern of the periodic WEC arrangement extends over length L in the y direction. There exists a cutoff frequency, below which oblique wave modes do not propagate, corresponding to a wavelength of $2L$ in general, or L if the WEC geometry and motion are also symmetrical about the O-x-z plane (see, e.g., Ref. [33]). Hereafter, the excitation frequency is assumed to be lower than the cutoff frequency.

Most typically, the WEC arrangement pattern consists of a single WEC, so that L would correspond to the distance between the gravity centers of two consecutive WECs, as in the illustration of Fig. 1 (a), but one could also imagine groups of WECs of various shapes, periodically repeated, as in Ref. [34]. Linear potential theory is assumed, allowing the decomposition of the hydrodynamic problem into a diffraction problem (where the devices are assumed to be fixed in the incident wave) and a radiation problem (where the devices undergo forced unitary motion, in otherwise still water).

For a unit incident potential propagating along the positive x axis, the far-field solution takes the form of plane waves, as x tends to both positive and negative infinities. In other words, regardless of the precise solution in the vicinity of the WECs, the WEC-wave interaction results in a reflected plane wave, propagating backward towards negative x, and a transmitted plane wave, propagating forward towards the positive x axis. From the linearity of the problem, reflected and transmitted waves are related to the incident wave through a multiplication by complex reflection and transmission coefficients, respectively, denoted as $\hat{r}$ or $\hat{R}$ and $\hat{t}$ or $\hat{T}$, where lowercase notations are employed for fixed devices, while capital letters are employed for oscillating devices.

The core of the present approach consists of representing the transmission coefficient in the complex plane. As seen in the next sections, the location of $\hat{t}$ and $\hat{T}$ satisfies a number of geometrical properties related to the fundamental properties of WECs in general. Furthermore, the choice of WEC control parameters allows tuning the location of $\hat{T}$, while remaining within the set of physically allowable values.

B. Fixed devices

First consider the devices fixed—noting that, because of the WEC symmetry with respect to the O-y-z plane, the reflection coefficient is identical, regardless of whether the incident wave propagates forward or backward. Without solving for the particular diffraction problem considered, simple relationships can be deduced from first principles. Since there is no source of energy dissipation or absorption at the WEC level, preservation of energy implies

$$|\hat{r}|^2 + |\hat{t}|^2 = 1. \tag{1}$$

Now consider two unit incident waves, one propagating backward and the other one forward. The total wave propagating away from the device, in the backward x direction, is the sum of the reflection from the forward incident wave, and the transmission from the backward incident wave. Similarly, the wave propagating away from the devices, in the forward direction, is the sum of the transmission from the forward incident wave and the reflection from the backward incident wave. Thus, preservation of energy implies

$$|\hat{r} + \hat{t}|^2 = 1. \tag{2}$$

Together with Eqs. (1) and (2), it is implied that $\mathrm{Re}\{\hat{t}\hat{r}^*\} = 0$, i.e., $\hat{r}$ and $\hat{t}$ are orthogonal. Visualized geometrically in the complex plane, $\hat{t}$ and $\hat{r}$ form the two sides of a right triangle with unit hypotenuse, see Fig. 2. Both $\hat{t}+\hat{r}$ and $\hat{t}-\hat{r}$ belong to the unit circle.

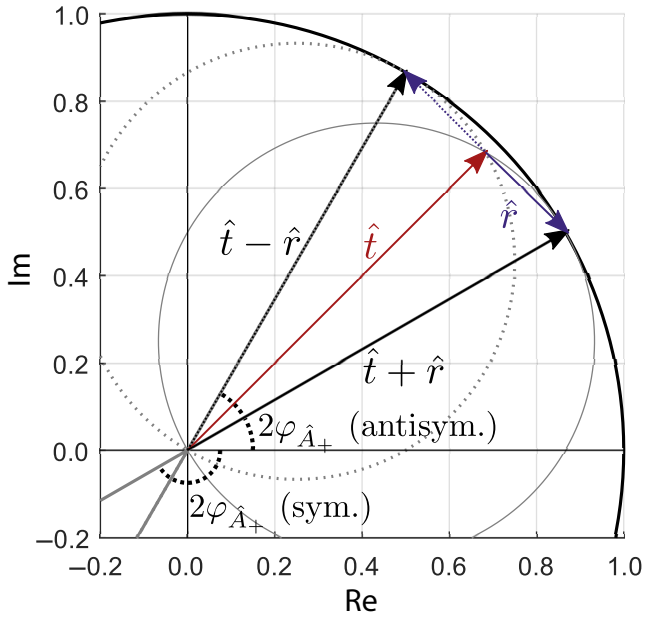

FIG. 2. Geometrical representation of transmission and reflection coefficients for a row of fixed structures, from Eqs. (1), (2), and (4).

Broadly speaking, obstacles with a larger horizontal characteristic dimension in the y direction, i.e., with a greater "blockage ratio," would be expected to reflect more. In addition, the row is generally more transparent to larger wavelengths, so that $|\hat{t}|$ decreases, and $|\hat{r}|$ increases, as the wave frequency increases, except for the pathological case where the row is a wall reflecting the incoming wave entirely.

C. Forced oscillations

In the radiation problem, the devices undergo forced oscillations with velocity amplitude $\hat{v}$, in their single degree of freedom, in an otherwise undisturbed fluid. In the far field, those forced oscillations result in radiated plane waves with complex potential amplitudes, $\hat{\phi}^+_{\mathrm{rad}} = \hat{A}_+\hat{v}$, propagating forward in the positive x direction, and $\hat{\phi}^-_{\mathrm{rad}} = \hat{A}_-\hat{v}$ propagating backward in the negative x direction, with $\hat{A}_- = \hat{A}_+$ for symmetric modes of motion [Figs. 1(b) and 1(c)], and $\hat{A}_- = -\hat{A}_+$ for antisymmetric modes of motion [Figs. 1(d)–1(f)]. $\hat{A}_+$ and $\hat{A}_-$ are related to $\hat{t}$ and $\hat{r}$ through Newman's relationship [31], which is as follows:

$$\hat{A}_- + \hat{A}^*_-\hat{r} + \hat{A}^*_+\hat{t} = 0. \tag{3}$$

Equation (3) can be reformulated in a way that differs depending on whether the mode of motion is symmetric or antisymmetric:

$$\begin{aligned} \hat{t} + \hat{r} &= -e^{2j\varphi_{A_+}} \quad \text{(sym.)}, \\ \hat{t} - \hat{r} &= e^{2j\varphi_{A_+}} \quad \text{(antisym.)}, \end{aligned} \tag{4}$$

where $\varphi_{\hat{z}}$ denotes the angle of a complex number, $\hat{z}$.

Thus, in addition to the energy preservation properties of Sec. II B, Eq. (3) provides a relationship between the angle of the wave radiation coefficient, $\hat{A}_+$, and the fixed-case transmission and reflection coefficients, $\hat{t}$ and $\hat{r}$, respectively. A more precise meaning can now be given to the location of $\hat{t}$ and $\hat{r}$ in the complex plane. The energy preservation properties of Sec. II B and Newman's relationship, Eq. (3), can be summarized graphically in Fig. 2, for both symmetric and antisymmetric modes of motion.

In the forced oscillation problem, the fluid exerts a radiation force onto the device, proportional to the motion velocity amplitude, $\hat{v}$, which can be decomposed into inertial and damping terms as follows: $\hat{f}_{\mathrm{rad}} = (B_{\mathrm{rad}} - j\omega A_{\mathrm{rad}})\hat{v}$, where A_{rad} and B_{rad} are termed the radiation *added mass* and *damping* coefficients, respectively. The net average rate of energy transfer from the WECs to the fluid, over a cycle of oscillation, is found to be $P_{\mathrm{WEC}\to\mathrm{fluid}} = \frac{1}{2}B_{\mathrm{rad}}|\hat{v}|^2$. From preservation of energy, $P_{\mathrm{WEC}\to\mathrm{fluid}}$ must equal the power propagating away from the devices in the forward- and backward-propagating waves over a distance L of

the wave front, which implies the following relationship between B_{rad} and the amplitude of $\hat{A}_+$:

$$B_{\text{rad}} = 2\rho\frac{\omega^2}{g}c_g L|\hat{A}_+|^2, \tag{5}$$

where $c_g = \partial\omega/\partial k$ is the wave group velocity.

D. Freely moving devices

The WECs are now allowed to move under the effect of the incident wave. Let $\hat{e}$ denote the generalized excitation force for a unit incident potential propagating in the positive x direction. For symmetric modes of motion, $\hat{e}$ is identical, regardless of the wave propagation direction, whereas, for antisymmetric modes of motion, the excitation coefficient for a backward-propagating incident wave is $-\hat{e}$. The WEC equation of motion can be expressed in the frequency domain as follows:

$$\hat{Z}_m\hat{v} = \hat{e}, \tag{6}$$

where $\hat{Z}_m$ is the WEC complex mechanical impedance, which can be further detailed as $\hat{Z}_m = B_{\text{rad}} + j\,(-\omega(M + A_{\text{rad}}) + K/\omega)$, where M represents a mechanical inertia and K may represent any combination of hydrostatic and mechanical stiffness terms. Rewriting $\hat{Z}_m = B_{\text{rad}}(1 + j\,\gamma_m)$, the real parameter, γ_m, contains (normalized) inertial and stiffness terms and, in principle, can be tuned arbitrarily to any prescribed value, independently from the WEC hydrodynamic coefficients (i.e., radiation and excitation coefficients).

As the WECs are subject to the incoming wave excitation force, from the linearity of the problem, the total transmitted wave is the sum of the "fixed-case" transmitted wave and the wave radiated forward by the WEC motion and, similarly, the reflected wave is the sum of the fixed-case reflected wave and the wave radiated backward. Thus, the transmission and reflection coefficients, $\hat{T}$ and $\hat{R}$, respectively, can be expressed as follows:

$$\hat{T} = \hat{t} + \frac{\hat{e}\hat{A}_+}{B_{\text{rad}}(1 + j\,\gamma_m)},$$
$$\hat{R} = \begin{cases} \hat{r} + \frac{\hat{e}\hat{A}_+}{B_{\text{rad}}(1+j\,\gamma_m)} & \text{(sym. motion)}, \\ \hat{r} - \frac{\hat{e}\hat{A}_+}{B_{\text{rad}}(1+j\,\gamma_m)} & \text{(antisym. motion)}. \end{cases} \tag{7}$$

The only source of energy dissipation in the WEC dynamics described above is radiation damping. However, radiation energy is transferred back to the fluid in the form of radiated waves. Therefore, from a global point of view, energy preservation implies that $|\hat{T}|^2 + |\hat{R}|^2 = 1$, which should hold regardless of the choice of γ_m. The well-known Haskind's relationship [31] ensues (see Appendix A):

$$\hat{e} = \begin{cases} 2\rho\frac{\omega^2}{g}c_g L A_+ & \text{(sym.)}, \\ -2\rho\frac{\omega^2}{g}c_g L A_+ & \text{(antisym.)}. \end{cases} \tag{8}$$

As such, Haskind's relationship ensures energy preservation for devices moving freely under the effect of incident waves. Similarly to the fixed-case scenario, $\hat{T}$ and $\hat{R}$ form the two sides of a right triangle with unit hypotenuse, such that, regardless of the value of γ_m,

$$\hat{T} - \hat{R} = \hat{t} - \hat{r}\ \text{(sym.)}, \tag{9}$$
$$\hat{T} + \hat{R} = \hat{t} + \hat{r}\ \text{(antisym.)}. \tag{10}$$

The energy preservation properties highlighted above, together with Eq. (9), relating $\hat{T}$ and $\hat{R}$ to their fixed-case counterparts $\hat{t}$ and $\hat{r}$, are visualized geometrically in Figs. 3 and 4 for symmetric and antisymmetric modes of motion, respectively.

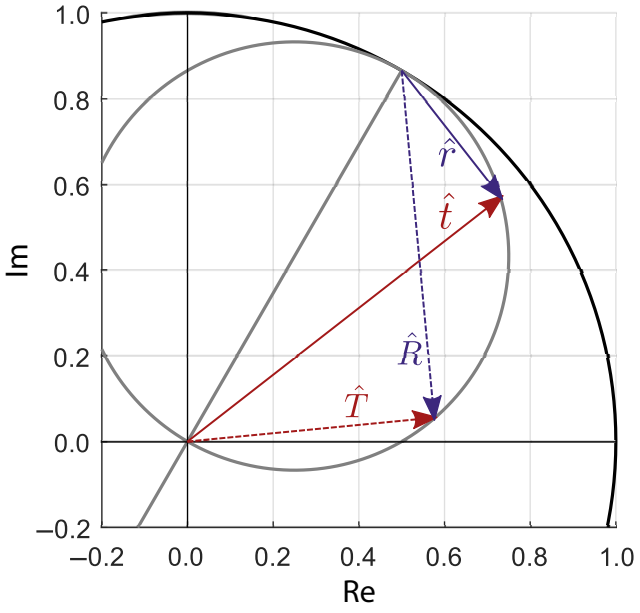

FIG. 3. Geometrical representation of reflection and transmission coefficients for a symmetric mode of motion.

III. CONTROL AND POWER ABSORPTION

In the following, the reflection and transmission coefficients are divided by $\hat{t} - \hat{r}$ (sym. case) or $\hat{t} + \hat{r}$ (antisym. case), which amounts to a simple phase shift, ensuring that the geometrical representation in the complex plane is located in the circle with center $\frac{1}{2}$ and radius $\frac{1}{2}$. These new coefficients are denoted as $\hat{r}'$, $\hat{t}'$, $\hat{R}'$, and $\hat{T}'$.

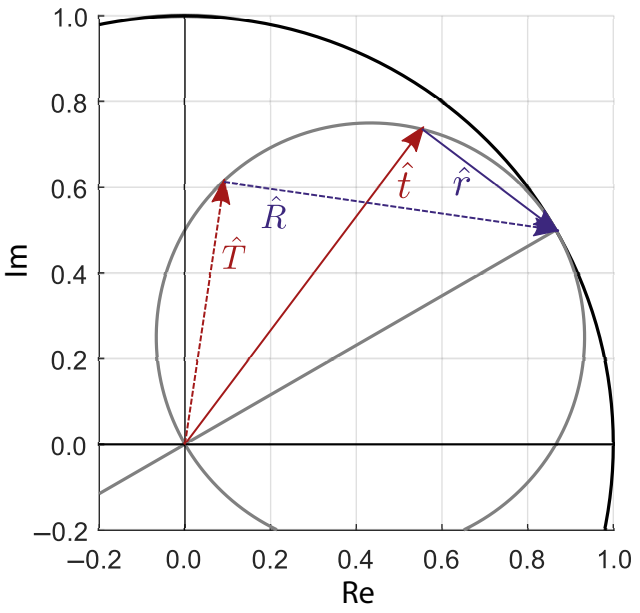

FIG. 4. Geometrical representation of reflection and transmission coefficients for an antisymmetric mode of motion.

A. Power absorption by unconstrained devices

For wave energy absorption, the mechanical energy of the WEC motion is converted into another form of energy, typically electric, through the PTO system, which exerts a force onto the device—see, for example, Ref. [35] for a review of wave-to-wire WEC models. WEC control essentially consists of adjusting the PTO system's behavior, to increase the average generated power. Control strategies range from a simple damping force, with an appropriately tuned coefficient, to sophisticated model-predictive control strategies with the ability to adjust the control force or WEC motion in real time, while satisfying force or motion constraints, and accounting for losses in the PTO system [13]. Here, the PTO force is modeled in the generic form of a combination of linear damping, stiffness, and inertia terms, as is commonplace in the wave energy literature, while bearing in mind the strong simplifications implied, with respect to state-of-the-art PTO models and control approaches [13,35]. Such parametrization is sufficient to achieve optimal power absorption under regular (single-frequency) waves, without motion constraints, through the celebrated "impedance-matching" (or "complex-conjugate") condition [18]. In fact, stiffness and inertia terms both contribute to tuning the WEC resonant frequency, so that those two parameters are redundant, and may be reduced to a single one, i.e., either stiffness or inertia [36].

The PTO action is thus represented by means of a control impedance, $\hat{Z}_u = B_u + j\,(-\omega M_u + K_u/\omega)$, where M_u, K_u, and B_u are the PTO inertia, stiffness, and damping, respectively. Regardless of the particular option retained for stiffness and inertia, it suffices to know that the imaginary part of the control impedance can be set to any prescribed value. Defining $\beta_u = B_u/B_{\text{rad}}$ as the normalized PTO damping, and $\gamma = (-\omega(M + M_u) + (K + K_u)/\omega)/B_{\text{rad}}$ as the normalized imaginary part of the total impedance, the WEC dynamics are now written as follows:

$$[1 + \beta_u + j\,\gamma]B_{\text{rad}}\hat{v} = \hat{e}, \tag{11}$$

where β_u can be set to any positive value (a negative PTO damping value would result in *providing* power to the wave field), and γ can be set to any value, positive or negative.

In a way similar to Sec. II D, and using Haskind's relationship, Eq. (8), the transmission coefficient, $\hat{T}'$, is found to be

$$\hat{T}' = \frac{1}{2} + \left(\frac{1}{2} - \hat{t}'\right)\frac{1 - \beta_u - j\,\gamma}{1 + \beta_u + j\,\gamma}. \tag{12}$$

For any row of WECs satisfying the assumptions in Sec. II, with a fixed-case transmission coefficient, $\hat{t}'$, Eq. (11) maps the choice of control impedance, reflected in the parameters β_u and γ, to the resulting transmission coefficient, $\hat{T}'$, in a way that is graphically visualized in Fig. 5 (where $\hat{t}'$ is chosen arbitrarily on the circle, C_0, to satisfy the properties highlighted in Sec. II). Straightforward algebraic manipulation of Eq. (11) shows that curves of $\hat{T}'$, for control impedance of the constant real part, map to

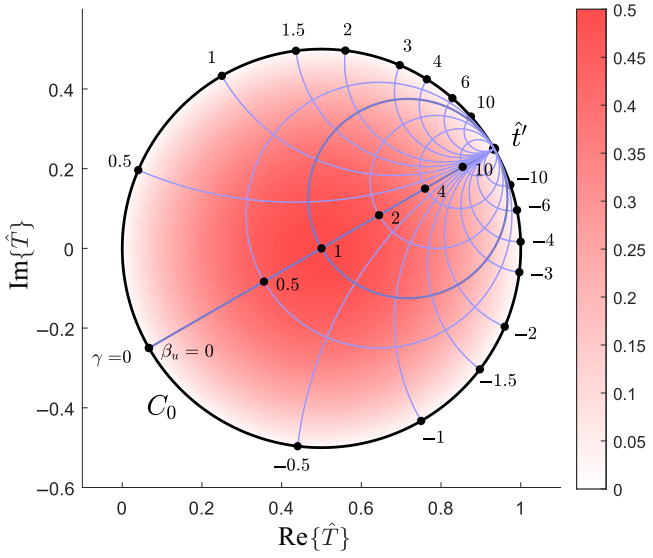

FIG. 5. Location of $\hat{T}'$ in the complex plane, depending on the real-valued normalized control parameters $\beta_u = B_u/B_{\text{rad}}$ and $\gamma = (-\omega(M + M_u) + (K + K_u)/\omega)/B_{\text{rad}}$, according to Eq. (11). Background color indicates the relative absorbed power, as in Eq. (12), between 0 (white) and 0.5 (red). Constant-β_u and constant-γ loci are represented for specific values of β_u and γ, which are labeled accordingly.

circles. Similarly, curves of $\hat{T}'$, for control impedance of the constant imaginary part, also map to circles. In addition, for a positive real part of the control impedance, $\hat{T}'$ is located inside the circle, C_0, of center $1/2$ and radius $1/2$. Those "constant-β_u" and "constant-γ" loci are represented in Fig. 5 for specific values of β_u and γ and labeled accordingly.

As seen clearly in Fig. 5, there is a one-to-one mapping between the choice of control impedance (with positive real part) and the location of $\hat{T}'$ in C_0. In principle, by appropriately tuning the two parameters of the control impedance, any transmission coefficient can be reached within the circle, C_0. As either β_u or γ tends to infinity, the transmission coefficient tends to its fixed-case value, $\hat{t}'$, as one would expect.

The incident power, available for each WEC of the row, can be calculated as the wave power across length L of the wave crest, that is, $P_w = \rho c_g L|\hat{\phi}_I|^2\omega^2/g$, for an incident potential with amplitude $\hat{\phi}_I$. Denoting the average mechanical power absorbed by each WEC as P_a, the *relative absorbed power*, or *hydrodynamic efficiency*, is simply calculated as $P_a/P_w = 1 - |\hat{T}'|^2 - |\hat{R}'|^2$, i.e., the fraction of the wave power that is neither reflected nor transmitted. Within the scope of the proposed graphical framework, P_a/P_w is given in a particularly simple manner as follows:

$$\frac{P_a}{P_w} = \frac{1}{2}(1 - 4d^2), \tag{13}$$

where d is the geometric distance between $\hat{T}'$ and the center of the circle, C_0, see Appendix B. Thus, it is easily verified that P_a/P_w takes values between 0 (when $\hat{T}'$ belongs to the circle) and 1/2 (when $\hat{T}'$ reaches the center of C_0), which is a well-known two-dimensional result for symmetric wave energy devices operating in one mode of motion [32]. The color map in Fig. 5 shows the relative absorbed power, depending on the location of $\hat{T}'$. Maximum relative power absorption occurs when $\hat{T}'$ is in the center of C_0, which requires two conditions: $\gamma = 0$ and $\beta_u = 1$. These two conditions amount to writing $\hat{Z}_u = \hat{Z}_m^*$, which is precisely the impedance-matching condition for WEC optimal power-maximizing control [17].

It can also be seen that, at resonance ($\gamma = 0$) but without control damping ($\beta_u = 0$), the roles of $\hat{T}'$ and $\hat{R}'$ are reversed, with respect to the fixed-case scenario. In addition, still keeping $\beta_u = 0$, there is a particular value of γ_u such that transmission is zero, and the whole incident wave is reflected.

B. Motion amplitude constraints

At first glance, it may seem surprising that the dimensions of the WECs constituting the row do not seem to enter into account in constructing Fig. 5. In particular, even arbitrarily small WECs can be made to absorb half the incident wave energy (if the PTO is set to the impedance-matching condition) or to reflect the incident wave entirely (for a well-chosen pure imaginary control impedance). To understand this apparent paradox, the motion amplitude associated with the different choices of $\hat{Z}_u$ should be considered. Reformulating Eq. (7) in terms of the velocity amplitude, $\hat{v}$, yields

$$\hat{v} = \frac{\hat{T} - \hat{t}}{\hat{A}_+} \tag{14}$$

which means that, at resonance, where $|\hat{T} - \hat{t}| = 1$ (see Fig. 5), the velocity amplitude is maximal, with a value of $|\hat{v}| = 1/|\hat{A}_+|$. Yet, it is clear that not all WEC geometries and modes of motion have the same wave-making ability, as represented by $\hat{A}_+$. For example, smaller WEC structures may have smaller values of $|\hat{A}_+|$, compared to larger structures with the same mode of motion. In general, the magnitude of $\hat{A}_+$, and therefore, the motion amplitude at resonance, are governed by the WEC dimensions and mode of motion: WECs that are poor wave makers require large amplitude motion to achieve resonance.

Large motion amplitudes violate the underlying assumptions of linear potential flow theory (which requires small motion) and may also be undesirable in practice. However, through appropriate tuning of the control parameters, one may seek to restrict the motion amplitude to a range of $|\hat{v}| \leq |\hat{v}|_{\max}$, where the maximum amplitude, $|\hat{v}|_{\max} = \sigma|\hat{\phi}_I|$, is expressed as a function of the incident potential amplitude by means of some proportionality coefficient, σ, in a way similar to Ref. [37]. Doing so, in effect, amounts to restricting the allowable transmission coefficients to the circular domain defined by $|\hat{T} - \hat{t}| \leq \sigma|\hat{A}_+|$, as exemplified in Fig. 6, which can always be achieved, e.g., by sufficiently increasing β_u.

Considering Fig. 6, Falnes' famous statement that "a good wave absorber must be a good wave maker" [38] becomes apparent: a row of WECs with good wave-making ability can achieve optimal wave power absorption through the impedance-matching condition, without reaching amplitude limits, while a row of WECs with poor wave-making ability can only achieve suboptimal power absorption, if its motion is to remain within reasonable bounds. Finally, Fig. 6 can also be seen as a particular case (for a single mode of motion and symmetric devices) of the results of Ref. [37] represented graphically using two-dimensional geometry.

IV. EXAMPLES

In this section, it is shown how specific WEC row hydrodynamic solutions can be visualized in the present geometrical framework. Two archetypal WEC types are considered in numerical examples: flap-type oscillating

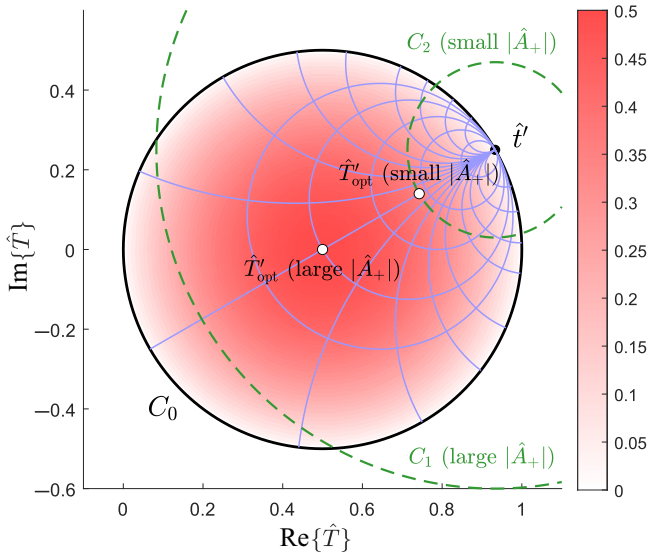

FIG. 6. Allowable $\hat{T}'$ in the complex plane, for WEC rows with good (intersection of C_0 and C_1) and lesser (intersection of C_0 and C_2) wave-making capabilities. In both cases, the best choice of $\hat{T}'$ to maximize power given the motion constraint is represented. For a WEC with small $\hat{A}_+$, complex-conjugate control under motion constraint cannot be achieved.

wave-surge converters and cylindrical heaving point absorbers.

A. Flap-type oscillating wave-surge converters

In this first example, the devices are rigid flaps, oscillating in pitch with their rotation axis on the sea bottom, aligned with the y direction. The flaps extend from the sea bottom to the surface, and they are assumed to be thin with respect to the wave's length. In the first case (flap 1), the flaps extend only over one fifth of the wave front ($W/L = 0.2$, where W is the width of each device), while, in a second case (flap 2), the flaps occupy half of the wave front ($W/L = 0.5$).

Assuming small motion and linear potential flow theory, the diffraction-radiation problem is solved using a matched eigenfunction expansion method, as in Ref. [39], which is an extension of the method used by Dalrymple and Martin for the diffraction problem only [40]. It is then assumed that, at each frequency, K_u and B_u are adjusted so that power absorption is maximized, while ensuring that the flap tip motion amplitude does not exceed that of the incident wave. At each frequency, instead of finding K_u and B_u explicitly, the optimized transmission coefficient, $\hat{T}'_{\text{opt}}$, is constructed geometrically, as in Fig. 6, from the fixed-case transmission coefficient, $\hat{t}'$, and the wave-making coefficient, $\hat{A}_+$. More specifically, the constraint on the tip motion is expressed as $h/\omega|\hat{v}| \leq \omega/g|\hat{\phi}_I|$, where h is the flap height (equal to the water depth), so that at each frequency the constraint is materialized through a circle centered around $\hat{t}'$, and with radius $\sigma|\hat{A}_+|$, where $\sigma = \omega^2/gh$.

The results are shown in Fig. 7. As can be expected from their relative sizes, the wave-making abilities of flaps 1 and 2 strongly differ [Fig. 7(a)]. In Figs. 7(b) and 7(c), the locus of the optimized transmission coefficient, $\hat{T}'_{\text{opt}}$, across the frequency range is represented. To illustrate the construction of each point of the locus, at three particular frequencies, ω_1, ω_2, and ω_3, the fixed-case transmission coefficient is shown (diamond-shaped markers), as well as the circles representing the motion constraint, which together allow the construction of $\hat{T}'_{\text{opt}}$ (circular markers), as explained in Sec. III B. For the row of flaps 1, motion constraints

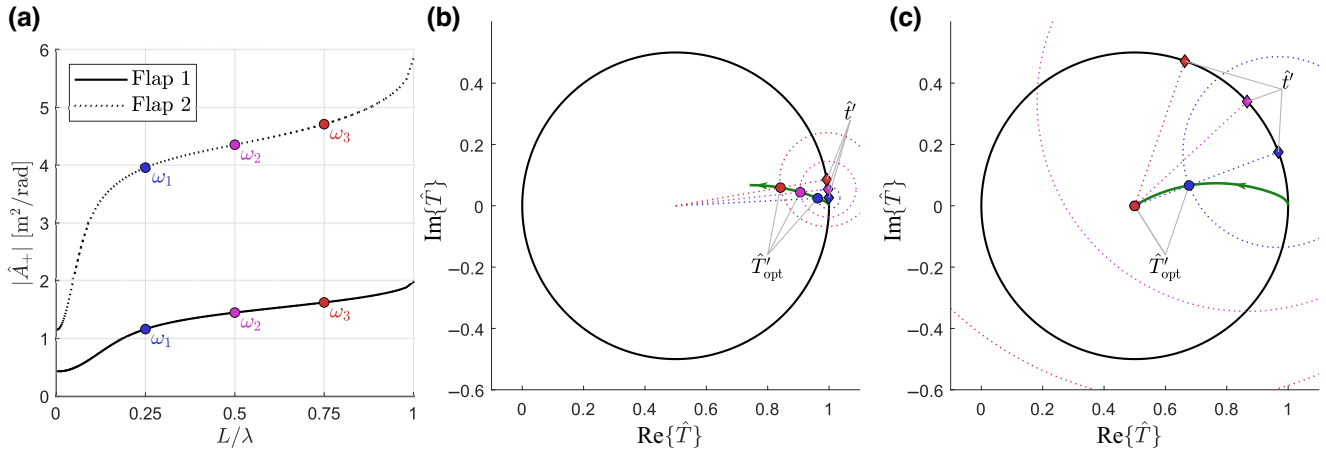

FIG. 7. Transmission-reflection properties of a periodic row of flap-type oscillating wave-surge converters, operating under constrained optimal control, spanning 1/5 (flap 1) and 1/2 (flap 2) of the transverse periodicity L. (a) Magnitude of the device's wave-making ability. Locus of the optimized transmission coefficient (green line) for a row of smaller (b) and larger (c) flaps, over the frequency range. In (c), optimal transmission coefficients at both ω_2 and ω_3 lie in the center of the circle. Arrow indicates the direction of increasing frequency. Dotted circles represent the motion constraint (see text).

confine the optimized transmission coefficient to a narrow area [Fig. 7(b)], relatively far from the unconstrained optimum. In contrast, above some frequency, ω, such that $L/\lambda \approx 0.4$, the row of larger flaps (flaps 2) can reach the unconstrained optimum for those frequencies, including in particular ω_2 and ω_3, $\hat{T}'_{\text{opt}} = 0.5$, and half of the incident wave power is absorbed [Fig. 7(c)].

B. Cylindrical heaving point absorbers

In this second example, the row consists of floating cylinders, with draft equal to 1/4 of the water depth (set to 10 m) and radius $R = 1$ m. The cylinders move, and absorb energy, in their heave mode of motion only. In the first case (cylinder 1), the row transverse periodicity is set to 5 times the cylinder diameter ($2R/L = 1/5$), while, in a second case (cylinder 2), the row transverse periodicity is set to 5/4 times the cylinder diameter ($2R/L = 4/5$). In other words, the row in the case named cylinder 2 is 4 times more densely populated in cylinders than in the case of cylinder 1.

The diffraction-radiation problem is solved following the method that can be found in Ref. [41], based on the construction of appropriate channel multipoles. Similarly to the flap cases, implementing the approach in Ref. [41] allows the determination of the fixed-case transmission coefficient, $\hat{t}'$, and the wave-making coefficient, $\hat{A}_+$, which suffice to construct $\hat{T}'_{\text{opt}}$ for each frequency. In this example, the motion constraint ensures that the vertical motion amplitude does not exceed the cylinder draft, in a unit amplitude incident free-surface elevation, which is expressed as $|\hat{v}| \leq \sigma|\hat{\phi}_I|$, with $\sigma = D\omega^2/g$ and D is the cylinder draft.

The results can be visualized in Fig. 8. Overall, the cylinders tend to exhibit more complex behavior than that of the flaps. In particular, from Fig. 8 (a), the relationship between the relative size of the cylinders (or row density), $2R/L$, and their wave-making ability is not straightforward. This increased complexity is also reflected in the locus of $\hat{T}'_{\text{opt}}$ over the frequency range [Figs. 8(b) and 8(c)]. Like in the previous example, the construction of $\hat{T}'_{\text{opt}}$ from $\hat{t}'$ and $\hat{A}_+$ is shown in more detail for three specific frequencies, ω_1–ω_3.

While the optimized transmission coefficient of the smaller cylinders is restricted to a relatively simple locus shape close to unity [Fig. 8(b)], that of the larger cylinders suggests more favorable power absorption capabilities in the lower-frequency range, together with complex changes in reflection-transmission properties [Fig. 8(c)]. Large reflection is observed, in particular, in the approximate range $\omega_1 \leq \omega \leq \omega_2$. The precise interpretation of such results would require a more thorough study of the diffraction-radiation solution for cylinders in a channel, which is beyond the scope of this article, but more on this rich subject can be found in Ref. [41] and references cited therein.

V. DISCUSSION AND CONCLUSION

Representing the WEC row transmission and reflection coefficients in the complex plane allows a straightforward visualization of many physical properties, most of which can be related to energy preservation considerations. Without power absorption, the transmission and reflection coefficients can be represented on the contour of a circular domain. Under controlled conditions, the PTO parameters allow the transmission coefficient to reach any prescribed value in the interior of the allowable circular domain, in principle. Absorbed power is maximal when the

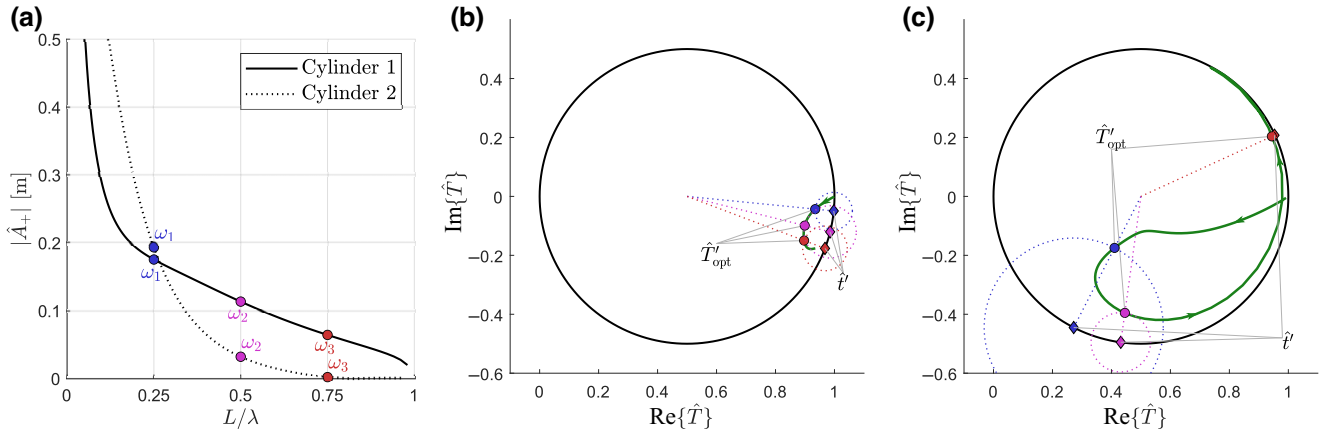

FIG. 8. Transmission-reflection properties of a periodic row of cylindrical heaving point absorbers, operating under constrained optimal control, with transverse row periodicity, L, equal to 5 (cylinder 1) and 5/4 (cylinder 2) times the cylinder diameter, $2R$. (a) Magnitude of the row wave-making ability. Locus of the optimized transmission coefficient (green line) for a row of cylinders of types 1 (b) and 2 (c), over the frequency range. Arrows indicate the direction of increasing frequency. Dotted circles represent the motion constraint (see text).

transmission coefficient is exactly in the center of the circular domain, which is achieved under the two well-known impedance-matching conditions, and decreases quadratically with the distance to the center. Motion amplitude limitations restrict the range of attainable transmission coefficients, all the more so for WECs with poor wave-making abilities.

A. Relation to the Smith chart

As mentioned in Sec. I, the proposed graphical representation, as summarized in Fig. 5, looks very similar to the Smith chart, an example of which is reproduced in Fig. 9. The Smith chart indeed represents the reflection coefficient of a transmission line, in the complex plane, depending on impedance parameters, namely, the length of the transmission line, on one hand, which governs the impedance imaginary part, and thus, is equivalent to our parameter γ, and the load, on the other hand, which is equivalent to our parameter β_u. The Smith chart is used as a visual aid to tune the line parameters to achieve impedance matching, which is also reached in the center of the circular chart.

However, there is not a strict analogy between the Smith chart and the present diagram for WEC analysis, because differences between the respective physical properties of the systems considered result in visual differences in the geometrical representations. In particular, in the Smith chart, the change in impedance can make reflection or transmission take any value in the unit circle, while, in the WEC-related physical problem, those coefficients are restricted to a smaller circle with radius 1/2 and a center, the location of which depends purely on the WEC geometry, through the fixed-case reflection and transmission coefficients. In addition, in the Smith chart, the circular arcs representing isolines of constant β_u values are horizontally aligned, unlike their WEC-related counterparts, which are aligned depending on the angle of the fixed-case coefficients. In a way, through the position of the fixed-case coefficients, there is more information present in the WEC-related geometrical framework. Finally, impedance matching in the Smith chart corresponds to a complete wave transmission, while, in the present work, impedance matching allows for absorbing half of the incident wave power.

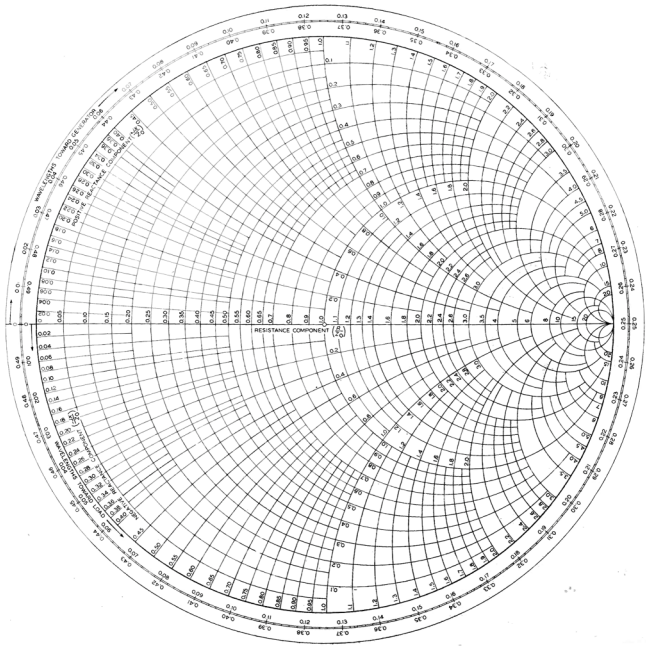

FIG. 9. Original version of the Smith chart, as printed in Ref. [28], for use as a graphical calculation tool.

B. Usefulness and limitations

WEC design and control are generally addressed with respect to power absorption maximization, without considering explicitly their impact on the surrounding wave field. The proposed geometrical framework is a step in that direction, by drawing a clear connection between WEC design, control, and wave reflection and transmission coefficients, under the simplifying assumptions detailed in Sec. II A. In particular, reflection and transmission eventually govern the WEC row interaction with previous and subsequent rows in a WEC farm, which can be modeled as outlined in Ref. [27]. Apart from possible modeling and design applications, there is certainly substantial didactic value in a concise visualization summarizing many fundamental physical properties of wave energy systems, as shown in Secs. II and III, in particular, the preservation of energy in the wave-structure interaction dynamics, Newman's and Haskind's relationships, and the conditions and values for maximal unconstrained and constrained power absorption.

In a single representation, as exemplified in Figs. 7 and 8, it is possible to visualize, for a given control strategy, how close the devices are to optimal power absorption, as well as their reflection and transmission behavior, across a prescribed frequency range. The examples in Sec. IV are obtained by assuming a specific control strategy, which requires only the determination of $\hat{t}'$ and $\hat{A}_+$ to represent the transmission coefficient under controlled conditions. In fact, only the scattering problem needs to be solved numerically, since $\hat{A}_+$ can be deduced from $\hat{e}$ through the Haskind relationship, and $\hat{e}$ is an output of the scattering solution. In general, though, knowing other hydrodynamic coefficients (A_{rad} and B_{rad}, in particular) remains essential to determine the value of the optimized control coefficients and to provide a comprehensive characterization of the WEC dynamics and forces.

The two examples selected demonstrate how apparently diverse WEC concepts can be incorporated into the proposed geometrical representation in a unified way, due to the fundamental hydrodynamic relationships common

to all WECs. Within this representation method, the two examples suggest that different geometries and modes of motion result in substantially different "signatures" of the transmission coefficient across the prescribed frequency range.

It would be interesting to examine how the proposed graphical representation can be enriched, when some of the simplifying assumptions are removed. In particular, the creation of vortices near the devices induces energy dissipation [42,43], i.e., energy that is neither transmitted back to the surrounding wave field nor absorbed by the PTO system. Therefore, in such a scenario, the energy preservation properties described in Secs. II B and II D should be amended, and the transmission coefficients should be moved to some location *inside* the circular domain. As yet, however, the precise effect of such nonlinear dissipation on the surrounding wave field has attracted little interest, to the best of our knowledge, and therefore, it is still unclear how exactly reflection and transmission coefficients would be affected, with respect to those of a "drag-free" scenario.

The present assumptions already cover a variety of WEC principles and arguably the most common ones (heaving point absorbers and oscillating wave-surge converters), as exemplified in Sec. IV. However, removing the symmetry assumption with respect to the O-y-z plane will be an interesting generalization of the present approach. In such a scenario, the device reflection coefficient and its wave-making abilities may differ, depending on whether the negative or positive x axis is considered. Additionally, in principle, the totality of the incoming wave energy may be absorbed [32]. Good examples are the famous "Salter's duck" or a wave paddle backed by a wall. Clearly, a different geometrical visualization is needed. Similar adaptations are required to represent reflection, transmission, and absorption properties of a WEC row with multiple degrees of freedom or an array consisting of multiple rows, which are both also able to capture all the incoming energy. In the latter case, however, the number of control parameters will be proportional to the number of degrees of freedom or to the number of rows, so that it will no longer be possible to draw a direct connection between a single pair of control coefficients (damping and stiffness) and a location in the complex plane, as is done herein.

Finally, the most challenging generalizations are probably those that would involve the presence of oblique propagating wave modes, and thus, would require a departure from a two-dimensional analysis of wave propagation. In particular, the consideration of a finite row, a modification of the incoming wave direction, incoming wavelengths smaller than the row periodicity, or the removal of the row periodicity assumption would all certainly make the analysis and visualization more challenging, but it would also be more representative of a real-sea scenario.

ACKNOWLEDGMENTS

The authors are grateful to Professor John Ringwood for bringing to our attention the Smith chart and pointing out its resemblance with our representation. This project has received funding from the European Union's Horizon 2020 research and innovation programme under Marie Skłodowska-Curie Grant Agreement No. 842967.

APPENDIX A: RELATIONSHIPS BETWEEN EXCITATION, RADIATION, AND WAVE-MAKING COEFFICIENTS

Starting with the energy preservation property, $|\hat{R}|^2 + |\hat{T}|^2 = 1$, $\hat{T}$ and $\hat{R}$ are replaced with their expressions given in Eq. (7). Also, using the fact that $|\hat{t}|^2 + |\hat{r}|^2 = 1$, and multiplying on both sides by $|1 + j\gamma_m|$, yields the following conditions:

$$\begin{aligned}
&\left|\frac{\hat{e}\hat{A}_+}{B_{\mathrm{rad}}}\right|^2 + \mathrm{Re}\left\{(\hat{t}^* + \hat{r}^*)\frac{\hat{e}\hat{A}_+}{B_{\mathrm{rad}}}(1 - j\gamma_m)\right\} = 0 \ \text{(sym.)},\\
&\left|\frac{\hat{e}\hat{A}_+}{B_{\mathrm{rad}}}\right|^2 + \mathrm{Re}\left\{(\hat{t}^* - \hat{r}^*)\frac{\hat{e}\hat{A}_+}{B_{\mathrm{rad}}}(1 - j\gamma_m)\right\} = 0 \ \text{(antisym.)}.
\end{aligned} \tag{A1}$$

These expressions take the form of first-order polynomials in γ_m, the coefficients of which must equate to zero, since energy preservation should remain valid, regardless of the value of γ_m. The following conditions ensue:

$$\frac{\hat{e}\hat{A}_+}{B_{\mathrm{rad}}} = \begin{cases} -(\hat{t} + \hat{r}) = e^{2j\varphi_{A_+}} & \text{(sym.)},\\ -(\hat{t} - \hat{r}) = -e^{2j\varphi_{A_+}} & \text{(antisym.)}. \end{cases} \tag{A2}$$

Also, using Eq. (5), the well-known Haskind relationship is found [31].

APPENDIX B: GEOMETRICAL REPRESENTATION OF POWER ABSORPTION

Using the fact that $\hat{T}' + \hat{R}' = 1$, one can write $\hat{T}'$ and $\hat{R}'$ as follows:

$$\begin{aligned}
\hat{T}' &= \frac{1}{2} + de^{j\phi},\\
\hat{R}' &= \frac{1}{2} - de^{j\phi},
\end{aligned} \tag{B1}$$

where $0 \le d \le 1/2$ is the geometrical distance of $\hat{T}'$ and $\hat{R}'$ to point $1/2$ (center of the circle, C_0).

The relative absorbed power is that which is neither transmitted nor reflected, i.e., $P_a/P_w = 1 - |\hat{R}'|^2 - |\hat{T}'|^2$, which yields, using the above parametrization, the

following:

$$P_a/P_w = \frac{1}{2}^2 + d^2 + 2d\cos\phi + \frac{1}{2}^2 + d^2 - 2d\cos\phi = \frac{1}{2}(1 - 4d^2), \tag{B2}$$

which is Eq. (12).

[1] A. Babarit, *Ocean Wave Energy Conversion: Resource, Technologies and Performance* (Elsevier, Amsterdam, 2017).

[2] D. R. David, A. Kurniawan, H. Wolgamot, J. E. Hansen, D. Rijnsdorp, and R. Lowe, Nearshore submerged wave farm optimisation: A multi-objective approach, Appl. Ocean Res. **124**, 103225 (2022).

[3] C. Nové-Josserand, F. C. Hebrero, L.-M. Petit, W.-M. Megill, R. Godoy-Diana, and B. Thiria, Surface wave energy absorption by a partially submerged bio-inspired canopy, Bioinspir. Biomim. **13**, 036006 (2018).

[4] J. Abanades, G. Flor-Blanco, G. Flor, and G. Iglesias, Dual wave farms for energy production and coastal protection, Ocean Coast. Manag. **160**, 18 (2018).

[5] C. Rodriguez-Delgado, R. J. Bergillos, M. Ortega-Sánchez, and G. Iglesias, Wave farm effects on the coast: The alongshore position, Sci. Total Environ. **640–641**, 1176 (2018).

[6] C. Xu and Z. Huang, A dual-functional wave-power plant for wave-energy extraction and shore protection: A wave-flume study, Appl. Energy **229**, 963 (2018).

[7] J. Abanades, D. Greaves, and G. Iglesias, Coastal defence using wave farms: The role of farm-to-coast distance, Renew. Energy **75**, 572 (2015).

[8] S. Narayan, M. W. Beck, B. G. Reguero, I. J. Losada, B. van Wesenbeeck, N. Pontee, J. N. Sanchirico, J. C. Ingram, G.-M. Lange, and K. A. Burks-Copes, The effectiveness, costs and coastal protection benefits of natural and nature-based defences, PLOS ONE **11**, e0154735 (2016).

[9] S. Zheng, A. Antonini, Y. Zhang, D. Greaves, J. Miles, and G. Iglesias, Wave power extraction from multiple oscillating water columns along a straight coast, J. Fluid Mech. **878**, 445 (2019).

[10] A. Bender, O. Langhamer, and J. Sundberg, Colonisation of wave power foundations by mobile mega- and macro-fauna – a 12 year study, Mar. Environ. Res. **161**, 105053 (2020).

[11] J. V. Ringwood, Wave energy control: Status and perspectives 2020, IFAC-PapersOnLine **53**, 12271 (2020).

[12] L. Wang, T. Zhao, M. Lin, and H. Li, Towards realistic power performance and techno-economic performance of wave power farms: The impact of control strategies and wave climates, Ocean Eng. **248**, 110754 (2022).

[13] N. Faedo, S. Olaya, and J. V. Ringwood, Optimal control, MPC and MPC-like algorithms for wave energy systems: An overview, IFAC J. Syst. Control **1**, 37 (2017).

[14] G. Bacelli, P. Balitsky, and J. V. Ringwood, Coordinated control of arrays of wave energy devices–benefits over independent control, IEEE Trans. Sustainable Energy **4**, 1091 (2013).

[15] P. B. Garcia-Rosa, G. Bacelli, and J. V. Ringwood, Control-informed optimal array layout for wave farms, IEEE Trans. Sustainable Energy **6**, 575 (2015).

[16] J.-C. Gilloteaux and J. Ringwood, Control-informed geometric optimisation of wave energy converters, IFAC Proc. Vol. **43**, 366 (2010).

[17] K. Budal and J. Falnes, *et al.*, Power generation from ocean waves using a resonant oscillating system, Mar. Sci. Commun. **1**, 269 (1975).

[18] K. Budal and J. Falnes, A resonant point absorber of ocean-wave power, Nature **256**, 478 (1975).

[19] L. Hai, M. Göteman, and M. Leijon, A methodology of modelling a wave power system via an equivalent rlc circuit, IEEE Trans. Sustainable Energy **7**, 1362 (2016).

[20] X. Garnaud and C. C. Mei, Bragg scattering and wave-power extraction by an array of small buoys, Proc. R. Soc. London A Math. Phys. Sci. **466**, 79 (2009).

[21] V. Rey, G. Arnaud, J. Touboul, and K. Belibassakis, Water wave scattering by dense or sparse arrays of surface-piercing bodies by integral matching method, Appl. Ocean Res. **75**, 132 (2018).

[22] G. Arnaud, V. Rey, J. Touboul, D. Sous, B. Molin, and F. Gouaud, Wave propagation through dense vertical cylinder arrays: Interference process and specific surface effects on damping, Appl. Ocean Res. **65**, 229 (2017).

[23] X. Hu and C. T. Chan, Refraction of Water Waves by Periodic Cylinder Arrays, Phys. Rev. Lett. **95**, 154501 (2005).

[24] A. G. Davies and A. D. Heathershaw, Surface-wave propagation over sinusoidally varying topography, J. Fluid Mech. **144**, 419 (1984).

[25] C. P. Berraquero, A. Maurel, P. Petitjeans, and V. Pagneux, Experimental realization of a water-wave metamaterial shifter, Phys. Rev. E **88**, 051002 (2013).

[26] L. Domino, M. Fermigier, and A. Eddi, Artificial resonant crystals for hydroelastic waves, Appl. Phys. Lett. **117**, 063701 (2020).

[27] A. Mérigaud, B. Thiria, and R. Godoy-Diana, A wide-spacing approximation model for the reflection and transmission of water waves over an array of vertical obstacles, J. Fluid Mech. **923**, A2 (2021).

[28] P. H. Smith, Transmission line calculator, Electronics **12**, 29 (1939).

[29] P. H. Smith, An improved transmission line calculator, Electronics **17**, 130 (1944).

[30] J. F. White, *High Frequency Techniques: An Introduction to rf and Microwave Design and Computer Simulation* (John Wiley & Sons, Hoboken, New Jersey, 2004).

[31] J. N. Newman, Interaction of waves with two-dimensional obstacles: A relation between the radiation and scattering problems, J. Fluid Mech. **71**, 273 (1975).

[32] D. V. Evans, Power from water waves, Annu. Rev. Fluid Mech. **13**, 157 (1981).

[33] C. M. Linton and D. V. Evans, The interaction of waves with arrays of vertical circular cylinders, J. Fluid Mech. **215**, 549 (1990).

[34] J. Falnes, Wave-power absorption by an array of attenuators oscillating with unconstrained amplitudes, Appl. Ocean Res. **6**, 16 (1984).

[35] M. Penalba and J. V. Ringwood, A review of wave-to-wire models for wave energy converters, Energies **9**, 506 (2016).

[36] R. H. Hansen, *Design and control of the powertake-off system for a wave energy converter with multiple absorbers*, Ph.D. thesis, Department of Energy Technology, Aalborg University (2013).

[37] D. Evans, Maximum wave-power absorption under motion constraints, Appl. Ocean Res. **3**, 200 (1981).

[38] J. Falnes, K. Budal, Wave power conversion by point absorbers, Norwegian Maritime Res. **6**, 2 (1978).

[39] D. Wang, S. Qiu, J. Ye, and F. Liang, Wave protection effect of periodic row of bottom-hinged flap-type wave energy converters, Trans. Tianjin Univ. **22**, 563 (2016).

[40] R. A. Dalrymple and P. A. Martin, Wave diffraction through offshore breakwaters, J. Waterway, Port, Coast., Ocean Eng. **116**, 727 (1990).

[41] C. Linton, D. Evans, and F. Smith, The radiation and scattering of surface waves by a vertical circular cylinder in a channel, Philos. Trans. R. Soc. London Ser. A: Phys. Eng. Sci. **338**, 325 (1992).

[42] G. F. Knott and M. R. Mackley, On eddy motions near plates and ducts, induced by water waves and periodic flows, Philos. Trans. R. Soc. London Ser. A, Math. Phys. Sci. **294**, 599 (1980).

[43] S. P. R. Czitrom, R. Godoy, E. Prado, A. Olvera, and C. Stern, Hydrodynamics of an oscillating water column seawater pump. Part II: Tuning to monochromatic waves, Ocean Eng. **27**, 1199 (2000).